AIAA AVIATION Forum
June 27-July 1, 2022, Chicago, IL & Virtual
AIAA AVIATION 2022 Forum

10.2514/6.2022-4070

Qualification of Ice Accretion Characteristics on a Wind Turbine Blade Model at High Liquid Water Content Levels Pertinent to Offshore Wind Turbine Icing Phenomena

Harsha Sista[1], Haiyang Hu[2], Linchuan Tian[3] , and Hui Hu[4]

Department of Aerospace Engineering, Iowa State University, Ames, IA, 50011-1096, USA

Abstract

Onshore and Offshore Wind Turbines installed in cold climates experience are subject to icing conditions regularly. The objective of this study is to replicate the conditions experienced by Offshore Wind Turbines in cold climates that are prone to icing events involving high Liquid Water Contents (LWC) and to study the icing physics surrounding this phenomenon. In the present study, an experimental investigation is performed in the Icing Research Tunnel available at the Iowa State University (ISU-IRT) to study the dynamic ice accretion process over a Wind Turbine blade model for high Liquid Water Content (LWC) values. Four cases were tested for Glaze and Rime ice conditions each, at LWC = 0.5 g/m^3, 1.0 g/m^3, 2.0 g/m^3, and 4.0 g/m^3 with a runtime of t = 600s, 300s, 150s, and 75s respectively to keep the total amount of accreted ice constant. The test cases were performed at a temperature of T = -5°C for Glaze Ice and T = -15°C for Rime ice. A high-speed imaging camera was used to capture the time evolution of the ice accretion process for each case. Runback towards the trailing edge is observed for the Glaze Ice condition along with the formation of rivulet structures, while most of the ice accretion happens around the leading edge for the Rime Ice condition. The qualification of the ice accretion characteristics for each case was done by performing a 3D scan of the iced wind turbine blade model. Various 2D cross-sections were then extracted from the 3D object to compare the ice characteristics along the spanwise length. Following that, the Maximum Combined Cross Section (MCCS) was calculated and compared for each case to understand the change in the accreted ice shape in relation to the LWC. The leading-edge ice thickness was found to decrease with an increase in the LWC, except for the condition of Rime Ice at LWC = 4.0 g/m^3.

Nomenclature

AoA	=	Angle of Attack
C	=	Chord length of the airfoil
LWC	=	Liquid Water Content
MCCS	=	Maximum Combined Cross Section
MVD	=	Median Volume Diameter of a droplet
V	=	Airflow velocity
t	=	time index during the ice accretion process
T	=	Temperature
x	=	spatial *x* coordinate of the airfoil
y	=	spatial *y* coordinate of the airfoil

[1] PhD Student, Department of Aerospace Engineering.
[2] Post-Doctoral Researcher, Department of Aerospace Engineering.
[3] Post-Doctoral Researcher, Department of Aerospace Engineering.
[4] Martin C. Jischke Professor, Department of Aerospace Engineering, AIAA Associate Fellow.

I. Introduction

The impact of fossil fuels on accelerating the timeline of climate change around the world has led to the development of renewable energy sources such as Wind, Solar, Hydro, etc., as a viable alternative. Among these, Wind Energy is one of the fastest-growing renewable energy sources in recent decades [1]. A study has shown that by 2030, over 20% of the United States energy demand can be met by wind energy alone. To satisfy this goal, there needs to be an increase in both the onshore and offshore installation of wind turbines [2]. Recently, offshore wind turbine installation has become the target of a higher volume of research because of its distinct advantages over its onshore counterpart: stronger offshore winds can result in greater productivity, the turbine size can be significantly larger, and offshore wind parks can be installed closer to major cities, reducing the transmission line length to deliver the power [3]. Therefore, the challenges of increased installation cost, higher repair charges, and the difficulty of year-round access to the site due to changing weather conditions can be balanced by conducting research into decreasing the downtime of these turbines [4]. Due to this increase in the demand and viability of wind energy, the installation of wind turbines in cold climate regions has also increased. In a study by Lehtomaki [5], it was found that the total power generated by wind turbines in cold climates was 127 GW at the end of 2015. However, 72%, 94%, and 19% of wind turbines suffer from icing events in North America, Europe, and Asia, respectively. This is the major challenge to the power-producing capacity overcome for cold climate wind turbines, both onshore and offshore. Ice accumulation on the surfaces of wind turbine blades can change their shapes and decrease their aerodynamic performance, which can account for up to 30% of the Annual Energy Production (AEP) [6], [7]. In addition, ice accretion can also accelerate the natural corrosion process. The maintenance of the turbine is also not easy in these conditions because access to the turbines can be severely constrained if the sea freezes over and ships are unable to get to the site. These are the major problems that need to be considered while talking about offshore wind turbines and their icing processes. Both types of wind turbines have their own challenges, but it is imperative to understand and develop anti/de-icing techniques tailored for them to mitigate the icing-induced damages and performance degradations to ensure safer and more efficient operation of the onshore and offshore wind turbines in cold climates.

The process of icing can be classified into three distinct types: in-cloud icing, precipitation icing, and frost [8]. In-cloud icing occurs when supercooled water droplets hit a surface that is below the freezing point of water and freeze upon impact. Precipitation icing happens during rainy or snowy conditions and is responsible for higher ice accretion rates, even though the temperature is relatively higher. The third type of icing is frost, which happens when water vapor directly solidifies on a cold surface. This phenomenon occurs when the atmospheric conditions are not too windy and is relatively rarely observed. Out of these three types, in-cloud icing is the most prevalent and widespread form of icing, which is why it has been the focus of aircraft and wind turbine icing studies for many decades.

For in-cloud icing, the Liquid Water Content (LWC) and Median Volume Diameter (MVD) of the droplets are the two most important external factors apart from the wind speed, temperature, and blade characteristics. Based on these characteristics, in-cloud icing is further divided into three types: rime ice, glaze ice, and mixed ice. Rime ice forms when supercooled water droplets impinge onto a cold surface and freeze directly upon impact at temperatures below -10°C. The LWC and MVD are usually small for rime ice, which forms as an opaque, milky layer. Glaze ice forms at warmer temperatures, above -10 °C, but still below the freezing point of water. The LWC and MVD are relatively high for this type of ice, and not all the ice immediately freezes upon impact, which causes a part of it to run back along the surface in the direction of the wind. It appears as a sheet of clear, smooth, and glassy ice and is more dangerous than rime ice. Mixed ice formation is a result of the combination of rime and glaze ice conditions when different freezing rates at different points on the surface can result in a temperature difference, which changes the dynamics of the impingement process. Therefore, it is an uneven process, and mixed ice accreted on a surface can be hard to remove.

In comparison to the extensive investigations to quantify ice accretion characteristics and to develop anti/de-icing systems for onshore wind turbine icing protection, much less can be found in the literature to examine the dynamic icing process over offshore wind turbines. However, ice accretion on marine vessels has been studied for a few decades, which provides a fair idea about the factors involved in offshore icing events. Icing on ships and other offshore structures is caused by a combination of atmospheric sources and sea spray. The design of the ship hull, the velocity of the wave against the ship, and the intensity and duration of the spray are some important factors to consider. Out of these, sea spray is the major cause, contributing between 50-90% of all marine icing, depending on the weather conditions [9], [10]. Waves impact upon the ship structures, which generates spray droplets. These droplets move against the direction of motion of the ship. The characteristics of the droplets generated in sea spray, such as the Liquid Water Content (LWC) and Median Volume Diameter (MVD), were studied extensively by Ryerson [11]. It was found that, in comparison to the typical atmospheric icing conditions studied for onshore wind turbines with the liquid water

content (LWC) levels being smaller than 2.0 g/m^3 (i.e., LWC < 2.0 g/m^3 for onshore wind turbines), the LWC levels for offshore wind turbine icing scenario was found to become significantly higher, i.e., the LWC levels can becoming as high as ~ 20.0 g/m^3 [12]due to the sea sprays. In addition, the sea sprays consist of salt water, with the percentage of salt varying from 0 ~ 4.0%, depending on the ambient conditions [13]. While understanding the effect of large droplet size with much higher LWC levels on the dynamic ice accretion process and characterizing the effects of the salinity of the water droplets on the ice accretion characteristics for offshore wind turbines are the broad objectives of the present study, we present the experimental results obtained by conducting a comprehensive icing tunnel testing campaign to examine the dynamic ice accreting process over the surface of a wind turbine blade model at high LWC levels in order to elucidate the underlying physics pertinent to offshore wind turbine icing phenomena.

II. Experimental Setup

The experimental study was performed in the unique Icing Research Tunnel available at Iowa State University (i.e., ISU-IRT in short), which is a newly refurbished, multifunctional icing research tunnel. As shown schematically in Figure 1, ISU-IRT has a test section with four optically transparent side walls and dimensions of 2.0m in length x 0.4m in width x 0.4m in height. It has a capacity of generating a maximum wind speed of 60 m/s and airflow temperature down to - 25ºC. An array of pneumatic atomizers/spray nozzles (H. Ikeuchi and Co., Flat Spray BIMV Series Nozzles) were installed at the entrance of the contraction section of ISU-IRT to generate the droplets. The ISU-IRT is currently capable of generating LWC up to 5.0 g/m^3. The LWC can be adjusted by changing the air and water pressure and the supplied flow rate. By using ISU-IRT, extensive icing and anti-/de-icing studies have been carried out in recent years for various engineering applications. Further information about the ISU-IRT can be found in Gao et al. [14].

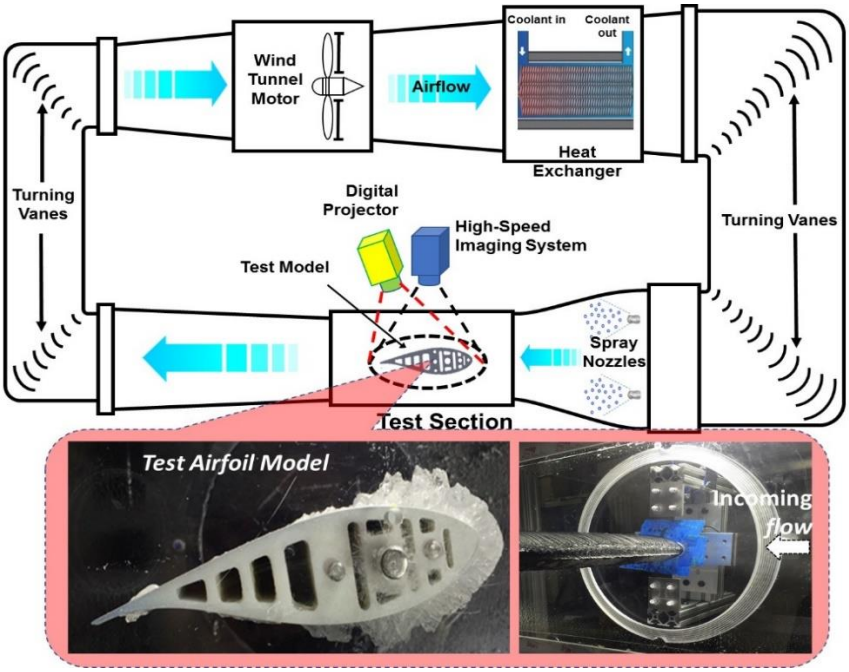

Figure 1: Schematic of the Iowa State University Icing Research Tunnel (ISU-IRT)

The airfoil model used in the experimental study is the DU91-W2-250 airfoil profile, which is widely used for wind turbine blade design due to its favorable aerodynamic performance and structural properties [15], [16]. The turbine blade model is 0.15m in airfoil chord length (i.e., C ¼ 0.15 m) and 0.40m in spanwise length. It was manufactured using a 3D printing rapid-prototyping machine. The surface of the model was sanded by using a series of progressively finer sandpapers, from 220 grit to 2000 grit, to achieve a smooth finish with a characteristic roughness of about 20-25μm [17]. Following that, several coatings of a primer were applied to prepare the surface for an all-weather spray-on enamel coating that is widely used to protect the surface of wind turbine blades (Rustoleum™, Flat

Protective Enamel, white in color). The blade was mounted using three stainless-steel rods and set at an Angle of Attack of 5.0 degrees (i.e., AOA=5.0°), which coincides with the angle at which the airfoil model has its maximum lift-to-drag ratio. To simulate typical Glaze icing conditions experienced by offshore wind turbines, the initial testing parameters were set to V_∞ = 40 m/s, T_∞ = -5 ºC. Typical Rime icing conditions experienced by offshore wind turbines were also simulated, with the initial testing parameters set to V_∞ = 40 m/s, T_∞ = -15 ºC. The ice accretion was studied for eight different test cases, as shown in Table 1:

Table 1: Test Matrix for the present study

Case Number	AoA (°)	V_∞ (m/s)	T (°C)	LWC (g/m^3)	Runtime (s)
1	5	40	-5	0.5	600
2	5	40	-5	1.0	300
3	5	40	-5	2.0	150
4	5	40	-5	4.0	75
5	5	40	-15	0.5	600
6	5	40	-15	1.0	300
7	5	40	-15	2.0	150
8	5	40	-15	4.0	75

To capture the ice accretion process over the wind turbine blade model, a high-resolution imaging system (Photron Fastcam Mini WX Series) was mounted normal to the airfoil chord of the wind turbine model. Low-flicker illumination was provided by a set of 150W fiber-coupled halogen lamps (RPS Studio CooLED 200 RS-5620). In addition, a Digital Image Processing (DIP)-based 3-D scanning system was used to capture the ice structure formed on the wind turbine model after running the experiment. The DIP system uses the concept of structured light triangulation in a similar fashion to the stereo vision technique, with one important difference: a digital projector replaces one of the cameras in the stereo pair. This projector highlights the accreted ice structures while the camera captures the surface characteristics.

III. Experimental Results and Discussion

Once the model was mounted inside the test section of the ISU-IRT, the spray nozzle system, already set at the desired Liquid Water Content, was switched on. The supercooled water droplets that are carried by the airstream impinge on the airfoil surface and begin accreting on the leading edge. Typical Glaze Ice conditions are simulated at V_∞ = 40 m/s and T = -5°C, with the formation of glassy, transparent ice structures that do not immediately freeze upon impact [18]. This happens because the heat transfer is insufficient to remove all of the latent heat of fusion released during the freezing process [19]. This unfrozen water is affected by the aerodynamic shear force exerted by the boundary layer airflow and starts moving towards the trailing edge, freezing in stages along the way [20]. Therefore, this runback results in the formation of rivulet structures. Typical Rime Ice conditions are also simulated at V_∞ = 40 m/s and T = -15°C, resulting in the formation of an opaque, milky white ice layer. In this case, the latent heat of fusion is easily removed by heat transfer, resulting in the supercooled water droplets freezing instantly upon impingement. This study attempts to establish how the ice accretion process for Glaze and Rime ice depends on the Liquid Water Content.

The high-speed imaging system captures the dynamic ice accretion process over the airfoil, out of which a slice is extracted and studied at various time instants to demonstrate the time evolution. Figure 2**Error! Reference source not found.** shows the dynamic ice accretion process for the Glaze icing condition at V_∞ = 40 m/s and T = -5°C at four different Liquid Water Contents: (a) LWC = 0.5 g/m^3, (b) LWC = 1.0 g/m^3, (c) LWC = 2.0 g/m^3 and (d) LWC = 4.0 g/m^3, with a runtime of 600s, 300s, 150s and 75s respectively:

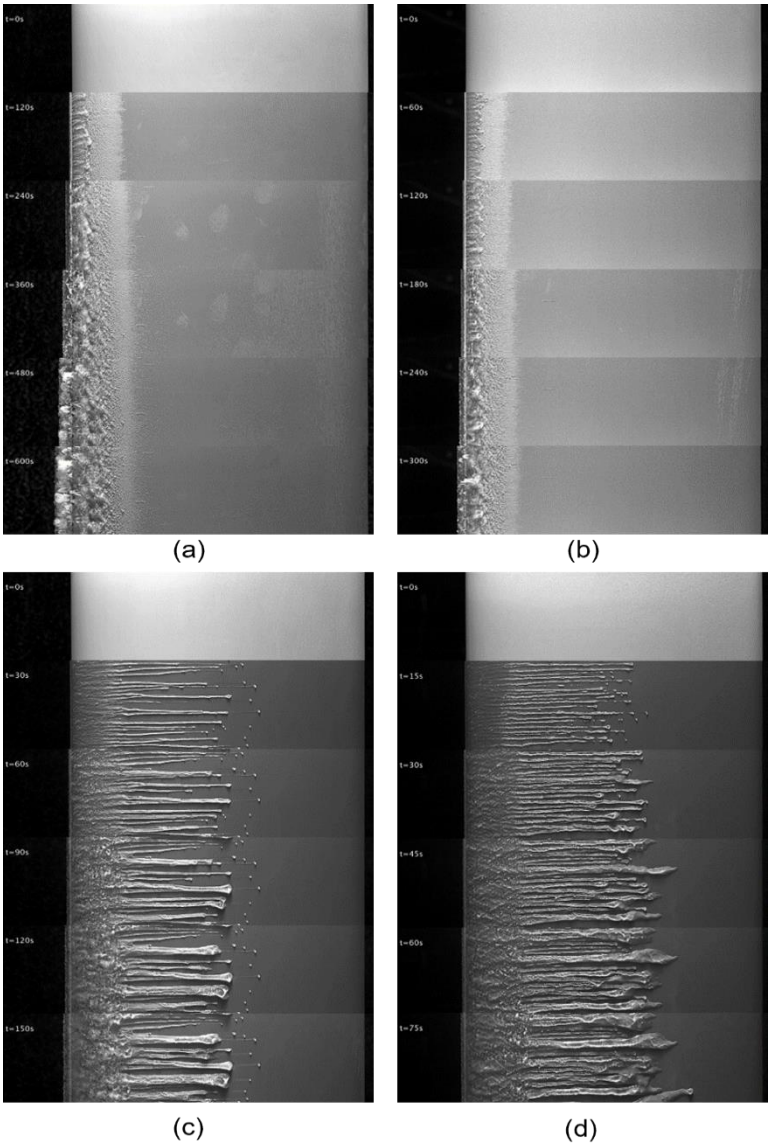

Figure 2: Dynamic Ice Accretion Process on the surface of the wind turbine blade model with V_∞ = 40 m/s, T_∞ = -5 °C and (a) LWC = 0.5 g/m^3 (b) LWC = 1.0 g/m^3 (c) LWC = 2.0 g/m^3 (d) LWC = 4.0 g/m^3.

From Figure 2**Error! Reference source not found.**(a), we can observe that for LWC = 0.5 g/m^3 and a runtime of 600 seconds, the glaze ice structure accretes rapidly on the leading edge, but there is not much runback. There is an initial stage of runback, where the impinged water does not instantly freeze. However, this process does not last long because the LWC is low, meaning that the latent heat of fusion is removed pretty quickly by heat transfer, although still not instantaneously. Following this, the ice directly begins accumulating on the leading edge, increasing the leading-edge ice thickness. The accreted ice has a clear and glassy structure, indicating that the ice formed is Glaze ice. From Figure 2(b), we can observe that for LWC = 1.0 g/m^3 and a runtime of 300 seconds, the glaze ice structure again forms majorly over the leading edge, with not much runback. The initial stage of runback is slightly greater, which decreases the ice thickness on the surface of the airfoil. In addition, the leading-edge ice thickness at the end of the process is lesser than case (a), showing that the ice is spread over more of the airfoil surface. However, a higher LWC value is needed to observe consistent runback spread across the airfoil. From Figure 2(c), we can observe that for LWC = 2.0 g/m^3 and a runtime of 150 seconds, the runback process is much more clearly visible, indicating that the latent heat of fusion is insufficiently dissipated by heat transfer, causing the droplets to remain in the liquid state for longer periods of time. This causes the liquid droplets to runback in the direction of the air stream and combine

with other droplets to form rivulet structures that are roughly evenly spaced along the spanwise direction. Once the runback freezes into clear, glassy structures, the leading-edge ice thickness starts increasing but is much lesser than in the previous cases. From Figure 2(d), we can observe that for LWC = 4.0 g/m^3 and a runtime of 75 seconds, the glaze ice structure is almost completely in the form of runback, indicating that the latent heat of fusion for this case is much higher than the heat transfer is capable of dissipating. Therefore, the runback reaches more than 50% of the chord length, and the small rivulets merge into larger, thicker structures closer to the trailing edge. Since most of the ice distribution is in the form of runback, the leading-edge ice thickness does not grow much throughout the process. In addition, since the time period for this case is only 75s, not all the ice that is pooled near the end of the runback structures changes into ice. Therefore, we can see that as the LWC increases, the latent heat of fusion generated by the icing process also increases, resulting in a greater region of runback and a lesser leading-edge ice thickness.

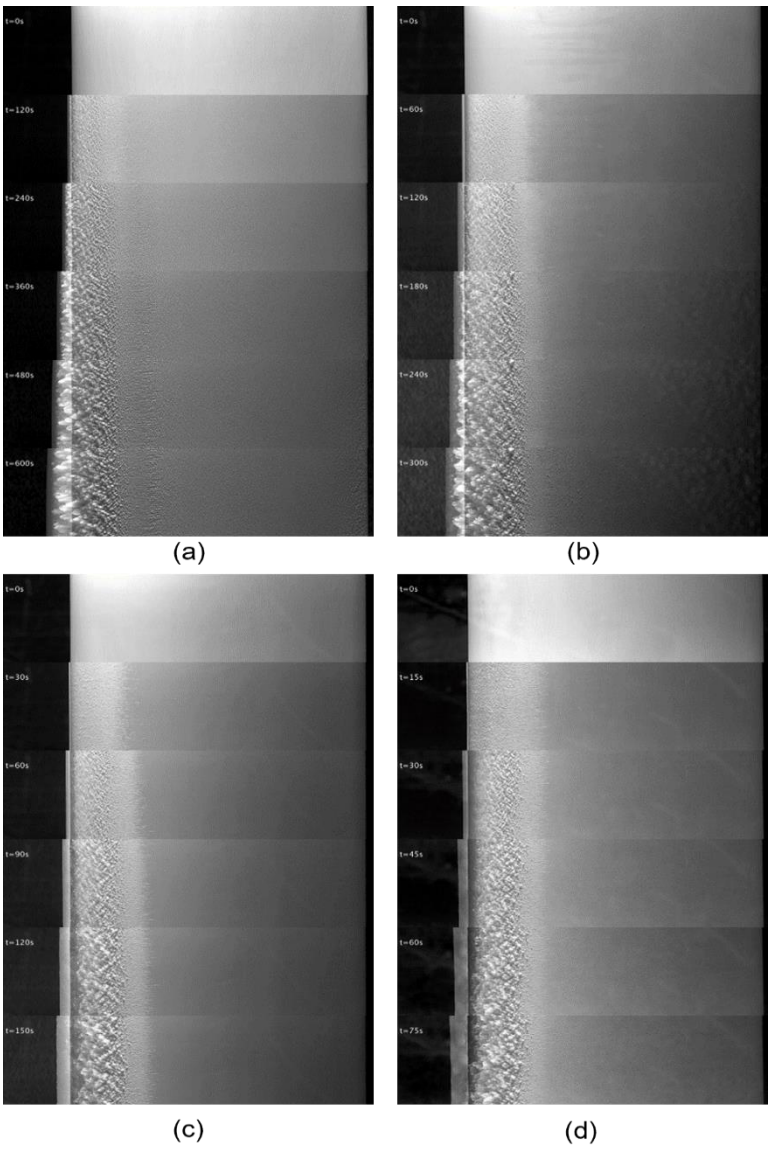

Figure 3: Dynamic Ice Accretion Process on the surface of the wind turbine blade model with V_∞ = 40 m/s, T_∞ = -15 °C and (a) LWC = 0.5 g/m^3 (b) LWC = 1.0 g/m^3 (c) LWC = 2.0 g/m^3 (d) LWC = 4.0 g/m^3

Figure 3 shows the dynamic ice accretion process for the Rime icing condition at V_∞ = 40 m/s and T = -15°C at four different Liquid Water Contents: (a) LWC = 0.5 g/m^3, (b) LWC = 1.0 g/m^3, (c) LWC = 2.0 g/m^3 and (d) LWC = 4.0 g/m^3, with a runtime of 600s, 300s, 150s and 75s respectively. From Figure 3(a), for LWC = 0.5 g/m^3 and a runtime

of 600 seconds, we can observe that the expected rime ice structure is formed, with all the supercooled droplets freezing immediately upon impact into an opaque, milky deposit. This means that the latent heat of fusion is taken away quickly by heat transfer due to the ambient temperature being so low. For a low LWC, all the droplets initially freeze near the leading edge, changing the shape of the airfoil and causing the subsequent droplets to accrete on the already formed ice over the leading edge. This causes the leading-edge ice thickness to grow significantly with time. From Figure 3(b), for LWC = 1.0 g/m^3 and a runtime of 300 seconds, we can observe that the characteristic rime ice structure continues to accrete close to the leading edge, indicating that the supercooled water droplets freeze upon impact. There is more ice accreted on the surface of the airfoil as compared to the previous case since the higher LWC allows more droplets to impinge over the surface. This results in a slight decrease in the leading-edge ice thickness with respect to time. From Figure 3(c), for LWC = 2.0 g/m^3 and a runtime of 150 seconds, we can observe that the expected rime ice structure is formed near the leading edge, with the ice distribution spreading more across the surface of the airfoil as well. As time goes on and the leading-edge ice thickness increases, there is a small layer of ice at the very top that does not represent the typical opaque, milky white characteristics expected from rime ice. This is the beginning of the formation of a translucent mixed ice layer, where glaze and rime ice freeze in different fractions. From Figure 3(d), for LWC = 4.0 g/m^3 and a runtime of 75 seconds, we can observe that there is a departure from the expected rime ice structure. The initial images show that the impinged droplets freeze immediately upon impact, similar to the above three cases. However, when the ice starts accreting on the leading edge, the ice layer is translucent and not opaque, indicating that the ice formed is mixed ice. As the ice accretion process continues, irregular structures grow on the leading edge, indicating where the ice accretion follows the pattern of glaze ice, while the remaining part continues to exhibit behavior associated with rime ice. The formation of a predominantly mixed ice layer above the leading edge is not observed in any other case and can be expected to form for high Liquid Water Content values, such as the one investigated in this case.

The iced model was then transported to a cooling chamber where the 3D scanning equipment was set up. The model was placed on a rotating turntable, and scans were taken at every four degrees, resulting in an array of ninety 2D scans. These scans were then fused together to form a 3D object, which gives a qualitative representation of what the ice accretion looks like in different cases. Figure 4 compares the four Glaze ice cases, while Figure 5 compares the four Rime ice cases. We can clearly see that the airfoil shape changes considerably, which is bound to decrease the performance of the wind turbine blade, as described in more detail in Gao et al. [16].

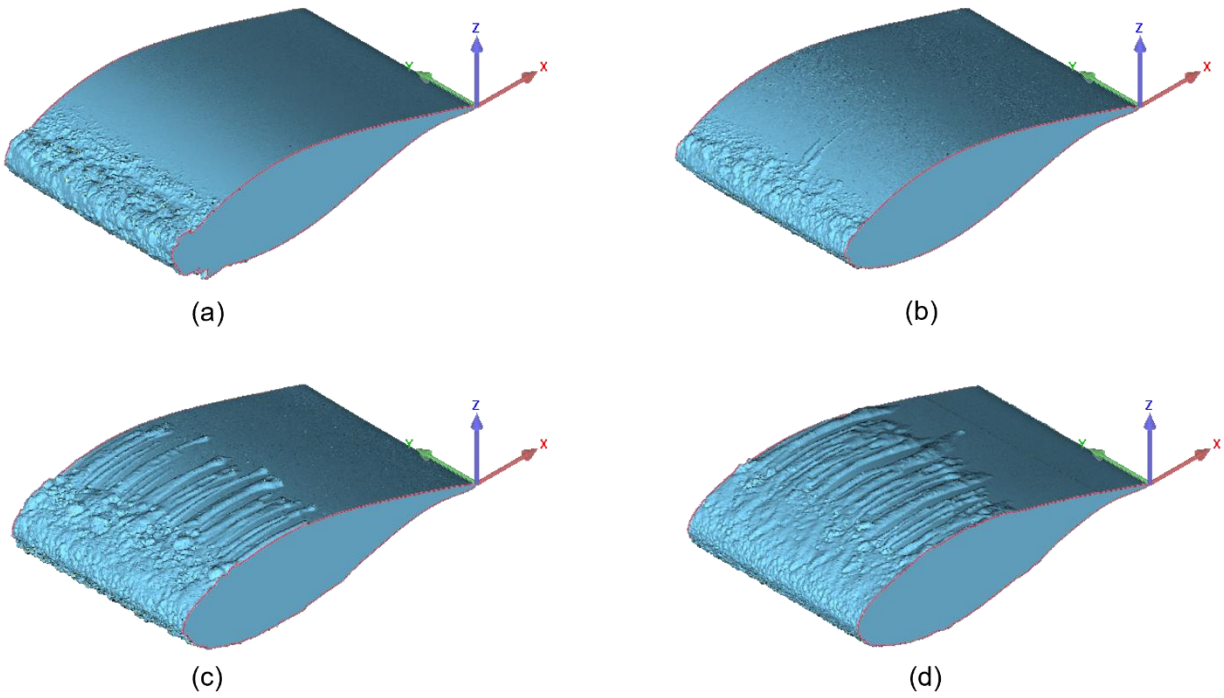

Figure 4: 3D Shape of the accreted ice on the surface of the wind turbine blade model with V_∞ = 40 m/s, T_∞ = -5 °C and (a) LWC = 0.5 g/m^3 (b) LWC = 1.0 g/m^3 (c) LWC = 2.0 g/m^3 (d) LWC = 4.0 g/m^3

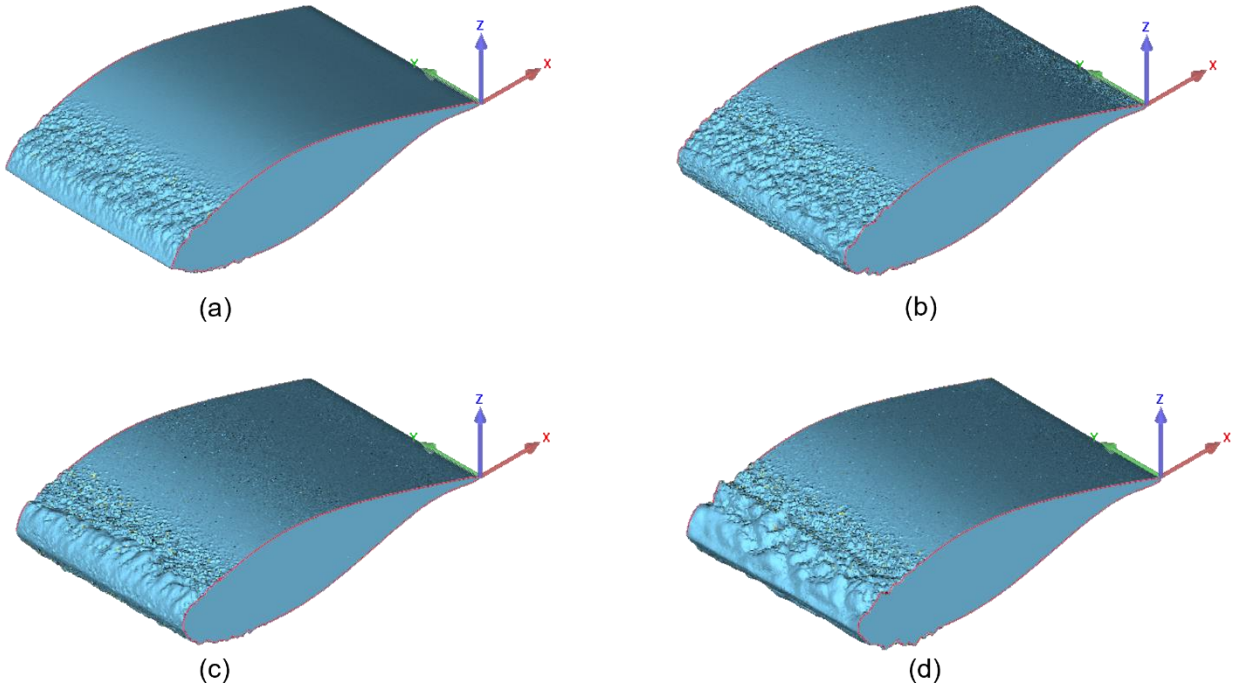

Figure 5: 3D Shape of the accreted ice on the surface of the wind turbine blade model with V_∞ = 40 m/s, T_∞ = -15 °C and (a) LWC = 0.5 g/m^3 (b) LWC = 1.0 g/m^3 (c) LWC = 2.0 g/m^3 (d) LWC = 4.0 g/m^3

From Figure 4, we can see more clearly how the runback increases with an increase in the Liquid Water Content for the glaze ice condition. For the LWC = 1.0 g/m^3 case in Figure 4(b), there are a couple of small rivulets formed in an otherwise uniform ice structure. This indicates that this value of LWC is the transition point after which rivulet formation can be observed. It is interesting to note that the rivulet formation is spread evenly across the span of the airfoil model, indicating a uniform ice accretion process, as shown in Figure 4(c) and Figure 4(d). In addition, the decrease of the leading-edge ice thickness with an increase in LWC can be clearly observed from the 3D scan results.

From Figure 5(a), we can see that the accreted ice is over the leading edge, forming a sharp, uniform edge. In Figure 5(b), there is more ice formed on the surface of the airfoil, and the sharpness of the leading-edge ice decreases. We observe this trend of the leading edge getting more rounded and the amount of ice formed on the airfoil surface increasing in Figure 5(c) as well. For the Rime ice condition at LWC = 4.0 g/m^3, the irregularities on the surface of the accreted ice are clearly visible, as seen in Figure 5(d). This formation of mixed ice increases the roughness of the surface and is also contrary to the smoothening trend observed in the previous three cases. Therefore, this adds to the belief that the formation of mixed ice at high LWC values is dangerous for offshore wind turbines in particular.

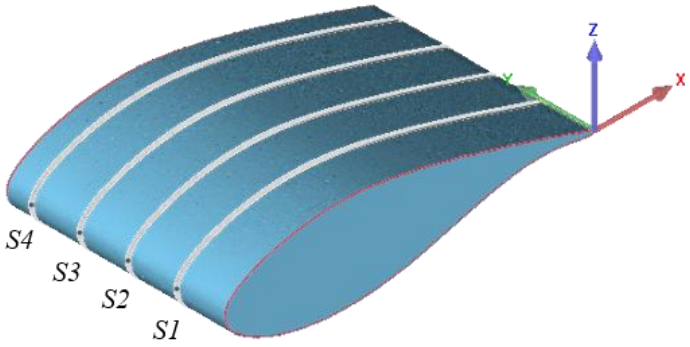

Figure 6: Positions of the Cross-Sections along the airfoil model span for extracting the 2D ice profiles

From these 3D objects, 2D slices are extracted at four different points along the spanwise direction to characterize the ice accretion shape more thoroughly and more quantitatively. These slices, labeled as S1, S2, S3, and S4, are taken at 20%, 40%, 60%, and 80% of the spanwise length, as shown in Figure 6 for the baseline case:

Each slice has been superimposed in the same coordinate plane and then compared with the non-iced wind turbine blade model, which is taken to be the baseline case. The slice coordinates have been normalized against the chord length C. Figure 7 shows the 2D ice structures for each of the four Glaze Ice cases, while Figure 8 shows the 2D ice structures for each of the four Rime Ice cases:

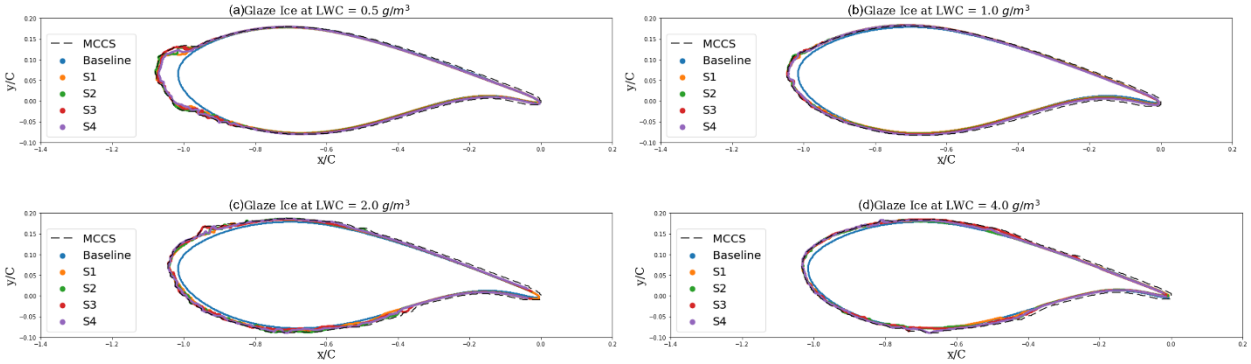

Figure 7: Comparison of 2D ice structures across various cross-sections of the model for Glaze Ice at (a) LWC = 0.5 g/m³ (b) LWC = 1 g/m³ (c) LWC = 2 g/m³ (d) LWC = 4 g/m³

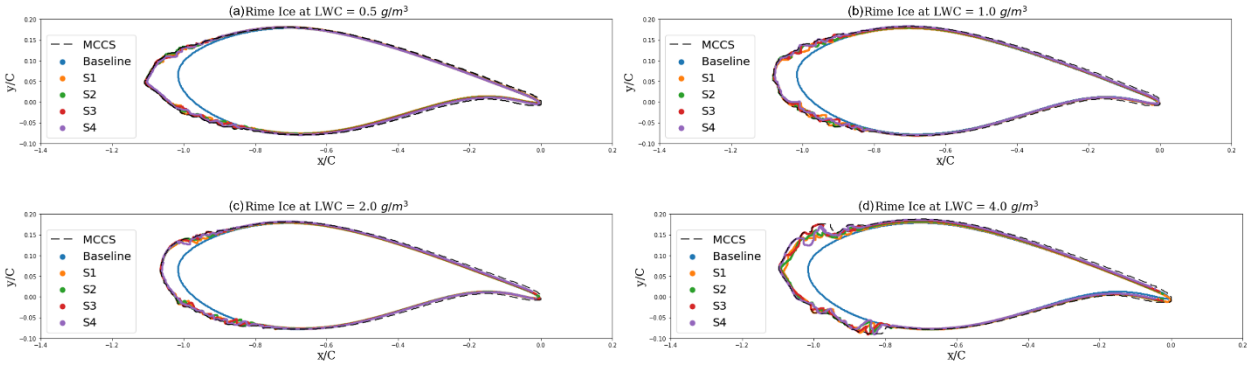

Figure 8: Comparison of 2D ice structures across various cross-sections of the model for Rime Ice at (a) LWC = 0.5 g/m³ (b) LWC = 1 g/m³ (c) LWC = 2 g/m³ (d) LWC = 4 g/m³

In general, we see that there is a good amount of overlap between the four slices, showing that the features of ice accretion for each case are fairly uniform along the spanwise length. However, there are also some differences between each slice, especially in the region beyond the leading edge, showing that the dynamic ice accretion process can never be truly uniform. The 2D slices give an additional quantitative insight into the variance of the dynamic ice accretion process with Liquid Water Content. From Figure 7, in the Glaze ice condition for LWC = 0.5 g/m^3, the ice accretes mostly around the leading edge. As the LWC increases, there is more ice over the surface downstream, which is indicative of runback. A similar trend is observed in **Error! Reference source not found.** for the Rime ice condition. However, there is a notable exception to this trend; the mixed ice case at LWC = 4.0 g/m^3, depicted in Figure 8(d). The irregularities that form due to different amounts of Glaze and Rime ice freezing at different points and in different fractions lead to the leading-edge ice thickness increasing instead of decreasing. In addition, there are also some prominent differences observed when the slices for case (d) are superimposed on top of each other due to the above-mentioned irregularities.

The concept of Maximum Combined Cross Section (MCCS), which is mentioned in Woodward et al. [21], is used to acquire a comparison of how the ice shape depends on the Liquid Water Content. The MCCS is obtained by taking

the maximum outer boundary profile from the superimposed 2D sections seen by the black dashed lines in Figure 7 and Figure 8. The MCCS can be considered to be the outermost level of ice accretion for each case. The MCCS from each of the four Glaze ice cases and each of the four Rime ice cases are then superimposed in a single graph, as shown in Figure 9:

From Figure 9(a), we can see that the leading-edge ice thickness for Glaze ice is the greatest for LWC = 0.5 g/m^3 and decreases consistently with an increase in the LWC. Therefore, we can say that there is an inverse relationship between the leading-edge ice thickness and the LWC for the Glaze Ice condition. From Figure 9(b), we can see that the leading-edge thickness for rime ice also decreases with an increase in LWC, up until a value of LWC = 2.0 g/m^3, with the LWC = 4.0 g/m^3 acting as an outlier due to the formation of mixed ice and the corresponding surface irregularities discussed above.

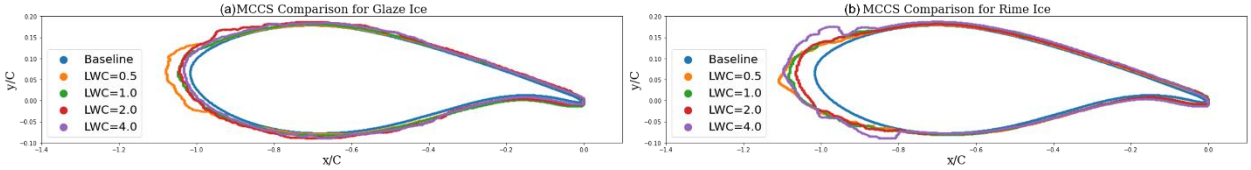

Figure 9: Comparison of the MCCS at different LWC levels for (a) Glaze Ice and (b) Rime Ice

IV. Conclusions

The research idea for the present study was to conduct a comprehensive experimental investigation to understand and elucidate the icing physics for high Liquid Water Content icing conditions. The experiments were conducted in the Icing Research Tunnel at Iowa State University (ISU-IRT), using the DU-91-W2-250 airfoil as the wind turbine model. 8 test cases were performed: 4 for Glaze ice and 4 for Rime ice at varying Liquid Water Contents. The dynamic ice accretion process for each case was captured using a high-speed imaging camera, and a 3D scanning system was also used to qualitatively visualize the ice structure formed for each case. 2D slices were extracted along the spanwise length and then superimposed over each other to visualize the ice thickness with respect to the non-iced baseline case. The Maximum Combined Cross Section (MCCS) was then calculated for each case, and the curves from the four glaze and four rime ice cases were compared to understand the relationship of ice accretion with respect to the Liquid Water Content. A decreasing trend in the leading-edge ice thickness was observed with an increase in the Liquid Water Content, for both Glaze and Rime ice conditions, with one notable exception, where mixed ice formation is observed. This qualification of the ice structure characteristics on a wind turbine blade model for high Liquid Water Content is helpful in improving our understanding of the icing events that are pertinent to Offshore Wind Turbines. This can, in turn, help with developing effective strategies to mitigate icing by creating anti/de-icing solutions that can adapt to these specific conditions.

Acknowledgments

The research work is partially supported by Iowa Energy Center for Wind Turbine Icing Study under the IEC Competitive Grant # 312350 and National Science Foundation (NSF) under award numbers of OISE-1826978, CBET-1916380, and TI-2140489.

References

[1] M. Grujicic, G. Arakere, B. Pandurangan, V. Sellappan, A. Vallejo, and M. Ozen, "Multidisciplinary design optimization for glass-fiber epoxy-matrix composite 5 MW horizontal-axis wind-turbine blades," *Journal of Materials Engineering and Performance*, vol. 19, no. 8, pp. 1116–1127, Nov. 2010, doi: 10.1007/S11665-010-9596-2/FIGURES/12.

[2] "20% Wind Energy by 2030: Increasing Wind Energy's Contribution to U.S. Electricity Supply", Accessed: Apr. 30, 2022. [Online]. Available: http://www.osti.gov/bridge

[3] S. P. Breton and G. Moe, "Status, plans and technologies for offshore wind turbines in Europe and North America," *Renewable Energy*, vol. 34, no. 3, pp. 646–654, Mar. 2009, doi: 10.1016/J.RENENE.2008.05.040.

[4] G. van Bussel, G. van Bussel, M. Zaaijer, and M. Sc, "Reliability, Availability and Maintenance aspects of large-scale offshore wind farms, a concepts study Characterisation and modeling of active and passive airfoil add-on's View project Reliability, Availability and Maintenance aspects of large-scale offshore wind farms, a concepts study," 2001, Accessed: May 01, 2022. [Online]. Available: https://www.researchgate.net/publication/239589238

[5] V. Lehtomäki, "Wind Energy in Cold Climates Available Technologies-report," 2016.

[6] F. Lamraoui, G. Fortin, R. Benoit, J. Perron, and C. Masson, "Atmospheric icing impact on wind turbine production," *Cold Regions Science and Technology*, vol. 100, pp. 36–49, Apr. 2014, doi: 10.1016/J.COLDREGIONS.2013.12.008.

[7] F. Feng, S. Li, Y. Li, and W. Tian, "Numerical simulation on the aerodynamic effects of blade icing on small scale Straight-bladed VAWT," *Physics Procedia*, vol. 24, pp. 774–780, Jan. 2012, doi: 10.1016/J.PHPRO.2012.02.115.

[8] O. Parent and A. Ilinca, "Anti-icing and de-icing techniques for wind turbines: Critical review," *Cold Regions Science and Technology*, vol. 65, no. 1, pp. 88–96, Jan. 2011, doi: 10.1016/J.COLDREGIONS.2010.01.005.

[9] S. Mintu, D. Molyneux, and D. Oldford, "State-of-the-Art Review of Research on Ice Accretion Measurements and Modelling," *Arctic Technology Conference 2016*, Oct. 2016, doi: 10.4043/27422-MS.

[10] T. Rashid, H. A. Khawaja, and K. Edvardsen, "Review of marine icing and anti-/de-icing systems," *https://doi.org/10.1080/20464177.2016.1216734*, vol. 15, no. 2, pp. 79–87, 2016, doi: 10.1080/20464177.2016.1216734.

[11] C. C. Ryerson, Ryerson, and C. C., "Superstructure spray and ice accretion on a large U.S. Coast Guard cutter," *AtmRe*, vol. 36, no. 3, pp. 321–337, 1995, doi: 10.1016/0169-8095(94)00045-F.

[12] S. A. Mintu, D. Molyneux, and B. Colbourne, "Ship-Wave Impact Generated Sea Spray: Part 1 — Formulating Liquid Water Content and Spray Cloud Duration," *Proceedings of the International Conference on Offshore Mechanics and Arctic Engineering - OMAE*, vol. 6A-2020, Dec. 2020, doi: 10.1115/OMAE2020-18223.

[13] G. F. N. Cox and W. F. Weeks, "Salinity Variations in Sea Ice," *Journal of Glaciology*, vol. 13, no. 67, pp. 109–120, 1974, doi: 10.3189/S0022143000023418.

[14] L. Gao, Y. Liu, L. Ma, and H. Hu, "A hybrid strategy combining minimized leading-edge electric-heating and superhydro-/ice-phobic surface coating for wind turbine icing mitigation," *Renewable Energy*, vol. 140, pp. 943–956, Sep. 2019, doi: 10.1016/J.RENENE.2019.03.112.

[15] W. A. Timmer and R. P. J. O. M. van Rooij, "Summary of the Delft University Wind Turbine Dedicated Airfoils," *Journal of Solar Energy Engineering*, vol. 125, no. 4, pp. 488–496, Nov. 2003, doi: 10.1115/1.1626129.

[16] R. P. J. O. M. van Rooij and W. A. Timmer, "Roughness Sensitivity Considerations for Thick Rotor Blade Airfoils," *Journal of Solar Energy Engineering*, vol. 125, no. 4, pp. 468–478, Nov. 2003, doi: 10.1115/1.1624614.

[17] L. Gao, Y. Liu, W. Zhou, and H. Hu, "An experimental study on the aerodynamic performance degradation of a wind turbine blade model induced by ice accretion process," *Renewable Energy*, vol. 133, pp. 663–675, Apr. 2019, doi: 10.1016/J.RENENE.2018.10.032.

[18] R. M. Waldman and H. Hu, "High-Speed Imaging to Quantify Transient Ice Accretion Process over an Airfoil," *https://doi.org/10.2514/1.C033367*, vol. 53, no. 2, pp. 369–377, Aug. 2015, doi: 10.2514/1.C033367.

[19] Y. Liu and H. Hu, "An experimental investigation on the unsteady heat transfer process over an ice accreting airfoil surface," *International Journal of Heat and Mass Transfer*, vol. 122, pp. 707–718, Jul. 2018, doi: 10.1016/J.IJHEATMASSTRANSFER.2018.02.023.

[20] K. Zhang, T. Wei, and H. Hu, "An experimental investigation on the surface water transport process over an airfoil by using a digital image projection technique," *Experiments in Fluids*, vol. 56, no. 9, pp. 1–16, Sep. 2015, doi: 10.1007/S00348-015-2046-Z/FIGURES/14.

[21] B. S. Woodard, A. P. Broeren, S. Lee, C. W. Lum, and M. B. Bragg, "Summary of ice shape geometric fidelity studies on an iced swept wing," *2018 Atmospheric and Space Environments Conference*, 2018, doi: 10.2514/6.2018-3494.